Intensity interferometry for the study of x-ray coherence

M. Yabashi*
SPring-8/JASRI, Mikazuki, Hyogo 679-5198, Japan

K. Tamasaku and T. Ishikawa†
SPring-8/RIKEN, Mikazuki, Hyogo 679-5148, Japan

(Received 30 September 2003; published 26 February 2004)

Intensity interferometry has been performed for the study of x-ray coherence. A high-resolution monochromator at $E=14.41$ keV was developed for enhancing the interference signal. Transverse coherence profiles of undulator radiation were evaluated from measurements of mode numbers. The obtained coherence length in vertical, which is perpendicular to the scattering plane of the monochromator, was proportional to the distance from the light source, as is expected from the Van Cittert–Zernike theorem. Vertical emittances of the storage ring were determined from the measured coherence lengths. Degradation of transverse coherence with phase object was measured and analyzed based on the propagation law of mutual intensity.

DOI: 10.1103/PhysRevA.69.023813 PACS number(s): 42.50.Ar, 41.50.+h, 07.85.Qe

I. INTRODUCTION

In the past decade, several important applications of coherent x rays have been developed. X-ray correlation spectroscopy [1–3] reveals dynamics of opaque samples. Propagation-based imaging techniques [4–7] enable to retrieve refractive phases of weakly absorbing materials with a simple optical system. Coherent diffraction method [8–11] would be used for a three-dimensional reconstruction of noncrystalline objects with an atomic resolution. Diffraction-limited nanofocused x rays, achieved under coherent illumination [12], will be a powerful probe for microscopic researches.

These developments are based on the progress of the third generation synchrotron sources, such as ESRF (France), APS (United States), and SPring-8 (Japan); time-averaged brilliance has been increased by several orders of magnitude with the use of undulator installed in a low-emittance storage ring. Furthermore, x-ray free-electron lasers (XFELs), combined with long undulators and low-emittance linacs, are being developed as the fourth generation synchrotron source in order to improve peak brilliance by several orders of magnitude [13–15].

Characterization of coherence properties is a crucial issue for all applications of coherent x rays. In particular, coherence propagation through various x-ray optics (reflective, refractive, and diffractive) should be much investigated both from theoretical and experimental aspects. Another important purpose of the study of x-ray coherence is to give feedback to the accelerator physics. When synchrotron radiation is used as a probe for diagnosing the electron beam, the resolution is fundamentally limited by the wave nature of radiation. For ultimate high-resolution diagnosis, therefore, it is desirable to use x rays as a *particlelike* probe, rather than to use visible light or soft x rays.

Coherence is measured by interferometry. In the x-ray region, several interferometric methods have been proposed and performed for the study of transverse [16–23] and longitudinal [24–26] coherences. However, the applicable fields have been still restricted. First reason is the limitations on available optical elements so as not to bring unwanted disturbance of x-ray wave field. Second is the requirement of extremely high stability of the whole optical system (typically within subangstrom path difference) during a measurement time in order to avoid temporal smearing of the interferogram.[1]

Intensity interferometry, which was first developed by Hanbury Brown and Twiss [27], can avoid above difficulties. Intensity interference is recorded as correlation (coincidence) of photoelectric signals from independent detectors. Thus one does not require special optics for interfering optical wave fields. Long term stability is also unnecessary, because time constant for measuring correlation is very short, possibly less than a nanosecond. Another distinct point of the method from the conventional amplitude interferometry is to measure the second-order coherence that reflects radiation nature.

All present x-ray sources, from x-ray tubes to synchrotrons, are categorized into chaotic sources from the viewpoint of the second-order coherence. In this case, intensity interference is observed as an *enhancement* of probability of photoelectric correlation, and can be simply associated with the modulus of the first-order coherence function [28]. Historically, an application of intensity interferometry to diagnosis of synchrotron radiation was first proposed by Shuryak [29]. Quantitative evaluation for the third generation synchrotron sources was made by Ikonen [30]. Experimental observation for synchrotron radiation was made by Kunimune *et al.* [31] and Gluskin *et al.* [32] for x rays, Takayama *et al.* [33,34] for soft x rays, and Tanabe *et al.* [35] for visible light.

*Electronic address: yabashi@spring8.or.jp
†Also at SPring-8/JASRI, Mikazuki, Hyogo 679-5198, Japan.

[1]Recent studies show that stability problem can be relieved by the use of intensity correlation technique (see Ref. [64]).

We have recently developed a system of x-ray intensity interferometry for the quantitative study of x-ray coherence [36–38]. Two issues had to be addressed. One was to match the longitudinal coherence length to the pulse width by the use of high-resolution monochromator in order to get a considerable enhancement of the correlation. Because typical pulse width in the third generation synchrotron sources is 10–100 ps, we needed to develop a monochromator with sub-meV bandwidth [36]. The other was high brilliance of light source required for improving a signal-to-noise ratio (SNR) within a reasonable measurement time. The brightest x-ray source at present, the 27 m undulator of SPring-8 [39], was employed at the early stage of our study. These experimental apparatuses, presented in Sec. III, have been employed to measure transverse coherence profiles, as shown in Sec. IV. The method has been applied to the diagnosis of the light source, as written in Sec. V. A short undulator, instead of the 27 m devise, was used as a light source for direct measurement of emittance of storage ring. In Sec. VI, we investigate coherence degradation by stationary phase objects. The experimental results were analyzed by the propagation law of mutual intensity with stationary transmittance amplitude functions.

II. PRINCIPLE

The first-order coherence function $\Gamma_{12}^{(1)}$ represents the space-time correlation in complex amplitudes of optical fields at two points as

$$\Gamma_{12}^{(1)}=\langle E^*(\mathbf{x}_1,t_1)E(\mathbf{x}_2,t_2)\rangle, \tag{1}$$

where $\langle\cdots\rangle$ means the ensemble average. Under the crossspectral purity condition [28], the function can be factorized into spatial and temporal parts,

$$\Gamma_{12}^{(1)}=J(\mathbf{x}_1;\mathbf{x}_2)\,\gamma(t_1;t_2), \tag{2}$$

where J is the transverse coherence function (the mutual intensity) and γ is the normalized longitudinal coherence function [i.e., $\gamma(t_1;t_1)=1$]. The complex coherence factor $\mu(\mathbf{x}_1;\mathbf{x}_2)$ is given by the normalization of the mutual intensity as

$$\mu(\mathbf{x}_1;\mathbf{x}_2)=\frac{J(\mathbf{x}_1;\mathbf{x}_2)}{\sqrt{J(\mathbf{x}_1;\mathbf{x}_1)J(\mathbf{x}_2;\mathbf{x}_2)}}. \tag{3}$$

The second-order coherence function $\Gamma_{12}^{(2)}$ relates to the intensity correlation as

$$\Gamma_{12}^{(2)}=\langle I_1I_2\rangle=\langle E_1^*E_2^*E_2E_1\rangle, \tag{4}$$

where E_i means $E(\mathbf{x}_i,t_i)$ $(i=1,2)$. For polarized, chaotic radiation, $\Gamma_{12}^{(2)}$ is written as

$$\Gamma_{12}^{(2)}=\langle I_1\rangle\langle I_2\rangle+|\Gamma_{12}^{(1)}|^2. \tag{5}$$

We consider to measure photoelectric coincidence count between two independent detectors for pulsed light. If we place a slit and a beam splitter in front of the detectors, the probability of coincidence count for the single pulse, P_{AB}, is given by

$$P_{\mathrm{AB}}=\frac{\eta_{\mathrm{A}}\eta_{\mathrm{B}}}{(\hbar\omega)^2}\int\int\int\int F_{\mathrm{S}}(\mathbf{x}_1)F_{\mathrm{S}}(\mathbf{x}_2)F_{\mathrm{T}}(t_1)F_{\mathrm{T}}(t_2)\times\Gamma_{12}^{(2)}d\mathbf{x}_1d\mathbf{x}_2dt_1dt_2, \tag{6}$$

where η_{A} and η_{B} are the quantum efficiencies, ω the central frequency of radiation, F_{S} the aperture function of the slit, and F_{T} the pulse envelop function. Now we assume that the slit aperture is a rectangular shape with widths of w_{x}(horizontal)$\times w_{\mathrm{y}}$(vertical), and the field intensity is homogeneous within the aperture. We also assume the pulse envelop function F_{T} and the modulus of the all first-order coherence functions (two transverse and one longitudinal) are in Gaussian distributions. Then Eq. (6) is written as

$$P_{\mathrm{AB}}=P_{\mathrm{A}}P_{\mathrm{B}}[1+(M_{\mathrm{x}}M_{\mathrm{y}}M_{\mathrm{t}})^{-1}], \tag{7}$$

where P_{A} and P_{B} are the probabilities of photoelectric count for each detector, M_{x} and M_{y} the transverse mode numbers, and M_{t} the temporal mode number given as [28,41]

$$M_{\mathrm{i}}=\left\{\frac{\sqrt{\pi}\sigma_{\mathrm{i}}}{w_{\mathrm{i}}}\,\mathrm{erf}\left(\frac{w_{\mathrm{i}}}{\sigma_{\mathrm{i}}}\right)-\frac{\sigma_{\mathrm{i}}^2}{w_{\mathrm{i}}^2}\left[1-\exp\left(-\frac{w_{\mathrm{i}}^2}{\sigma_{\mathrm{i}}^2}\right)\right]\right\}^{-1} \quad (i=x,y), \tag{8}$$

and

$$M_{\mathrm{t}}=\sqrt{1+\frac{s_{\mathrm{t}}^2}{\sigma_{\mathrm{t}}^2}}. \tag{9}$$

In above equations, $\mathrm{erf}(x)$ is the error function, σ_{x} and σ_{y} are the transverse coherence lengths (in rms), s_{t} is the pulse width in full width at half maximum (FWHM), and σ_{t} is the longitudinal coherence time given by

$$\sigma_{\mathrm{t}}=\frac{4\hbar\ln 2}{\Delta E}, \tag{10}$$

where ΔE is the energy bandwidth in FWHM of the incident beam [38].

Next we consider to accumulate the coincidence count during a time T for repeated pulses with a rate of f. We introduce the enhanced ratio of normalized coincidence, R, as

$$R=\frac{P_{\mathrm{AB}}}{P_{\mathrm{A}}P_{\mathrm{B}}}-1=\frac{C_{\mathrm{AB}}fT}{C_{\mathrm{A}}C_{\mathrm{B}}}-1, \tag{11}$$

where $C_{\mathrm{AB}}=P_{\mathrm{AB}}fT$ is the total coincidence count, and $C_{\mathrm{A}}=P_{\mathrm{A}}fT$ and $C_{\mathrm{B}}=P_{\mathrm{B}}fT$ are the total counts by each detectors. Then Eq. (7) is simply represented as

$$R=1/(M_{\mathrm{x}}M_{\mathrm{y}}M_{\mathrm{t}}). \tag{12}$$

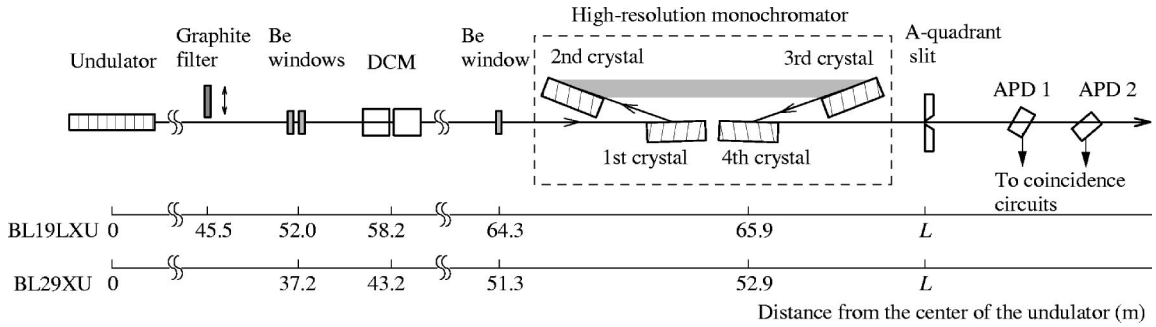

FIG. 1. Top view of the experimental setup. Undulator radiation ($\Delta E/E \gtrsim 10^{-3}$) is monochromatized with the double-crystal monochromator (DCM) using cryogenically cooled Si (111) [40] in $\Delta E/E \sim 10^{-4}$, and with the high-resolution monochromator (HRM) in $\Delta E/E \sim 10^{-8}$. The slit placed after the HRM adjusts beam size to the two avalanche photodiodes (APDs). The distances from the center of the undulator to the components for two beam lines are indicated below the figure, while those to the slit (L) appear in the text.

Equation (12) connects the coincidence enhancement R to the total mode number $M = M_x M_y M_t$; R tends to zero for the multimode limit ($M \to \infty$), while R increases to unity for the single-mode limit ($M \to 1$). This phenomenon known as the photon *bunching* effect is a characteristic nature of chaotic radiation. Practically, one has to keep M small to observe the effect. In particular, Eqs. (9) and (10) imply that we need to have monochromatic beam with sub-meV bandwidth in order to achieve small M_t for pulsed light with $s_t \sim 10$ ps.

The finite counting time introduces a statistical error ΔR in the measurement of R. The SNR in the multimode limit is given by

$$\frac{R}{\Delta R} \simeq \delta_s \overline{\eta} \sqrt{\frac{fT}{2}}, \tag{13}$$

where $\overline{\eta} = (\eta_A \eta_B)^{1/2}$ is the geometric mean of the efficiencies. The degeneracy parameter of the source, δ_s, is given by [42]

$$\delta_s \simeq \frac{\hat{B}_p \lambda^3}{4c}, \tag{14}$$

where $\hat{B}_p$ is the peak brilliance and λ the central wavelength. Equation (13) shows that high degeneracy (i.e., high peak brilliance) is required for achieving good SNR in a reasonable measurement time.

III. EXPERIMENT

Experiments were performed at the 27 m undulator beam line (19LXU) [43] and the 1 km beam line (29XU) [44] of SPring-8. During the measurement, the storage ring has been operated in the same filling pattern: $f = 37$ MHz with a minimum bunch separation of 23.6 ns. The peak brilliance at BL19LXU is $\hat{B}_p \sim 10^{23}$ photons/s/mm^2/mrad^2 in 0.1% bandwidth, which corresponds to a degeneracy of $\delta_s \sim 10^{-1}$ at $\lambda \sim 0.1$ nm.

The experimental setup is shown in Fig. 1. A high-resolution monochromator (HRM) is the key optics in order to raise the enhancement R. We found that extremely narrow bandwidth can be realized by the combination of four-bounced asymmetric reflections. From the analysis on the DuMond diagram, the bandwidth ΔE at a photon energy of E is approximately given by

$$\Delta E/E \simeq P b^{1.5} \omega_s \cot \theta_B, \tag{15}$$

where θ_B is the Bragg angle, P is the polarization factor given by 1 ($\cos 2\theta_B$) for σ (π) polarization, $b = \sin(\theta_B - \alpha)/\sin(\theta_B + \alpha)$ is the asymmetric factor for the first and second crystals ($1/b$ for the third and fourth crystals), and ω_s is a total reflection width for symmetric geometry. We chose Si (11 5 3) reflections with asymmetric angles of $\alpha = 78.4°$, which correspond to $\theta_B = 80.4°$, $b = 1/10.4$, and $\omega_s = 1.8$ μrad at $E = 14.41$ keV ($\lambda = 0.086\,03$ nm). Then Eq. (15) gives a theoretical resolution of $\Delta E \simeq 100$ μeV. Experimentally, the bandwidth has been determined to be $\Delta E = 120 \pm 15$ μeV from the measurement with nuclear forward scattering of ^{57}Fe [36].

A crucial issue is to assure preservation of transverse coherence through the HRM, while the asymmetric reflections change the transverse coherence in the scattering plane. Because our interest is to measure vertical coherence rather than horizontal one, the HRM crystals were aligned so as to give horizontal reflections (horizontal scattering planes, $P = 0.94$), which makes the vertical direction normal to the scattering plane. As a result, we can preserve vertical coherence even after the asymmetric reflections. The geometry also avoided limiting the spatial and angular acceptances in vertical direction.

A quadrant slit was placed after the HRM in order to change transverse mode numbers on detectors. As detectors, two avalanche photodiodes (APDs) [45] were arranged in tandem just after the last slit. The use of semitransparent APDs enabled to remove a beam splitting optic, which can decrease the efficiency. The inclination angles of the diodes to the beam axis were independently adjusted in order to increase detector efficiencies and to valance the counting rates between them. The mean efficiency $\overline{\eta}$ (including the HRM and detectors) was found to be around a few percent at $E = 14.41$ keV.

As shown in the previous sections, the ratio R can be determined by the total counting numbers C_{AB}, C_A, C_B, and the pulse number fT, if pulse heights are uniform and

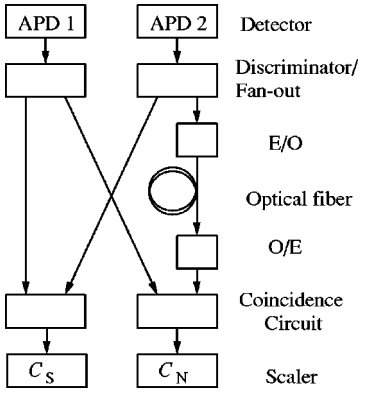

FIG. 2. Schematic of the coincidence circuit. The E/O, O/E converters, and the optical fiber produce a delay equal to the revolution period of the storage ring (4.79 μs). C_S is the true coincidence count. C_N is the accidental coincidence count used for the normalization of C_S.

unchanged. In a storage ring, however, beam currents of each bunch are unequal, and independently decay as a function of time. In this case, it is impossible to determine R only from the above parameters. To obtain R, we used a normalization technique presented in Ref. [31]. As seen in Fig. 2, the electric signal from each detector is split into two channels. One is to measure *true* coincidence count, $C_S = C_{AB}$, and the other is to measure *accidental* coincidence count, C_N. The latter is the coincidence between signals with the separation of a revolution period of the storage ring. Thus this does not reflect any coherence information. R is finally given by

$$R = C_S/C_N - 1, \tag{16}$$

with an assumption that change of intensity in the revolution period is neglected. The electrical delay circuit used in the early stage has been replaced later by the optical delay system in Fig. 2 in order to decrease the dead time in the delay circuit.

IV. MEASUREMENT OF TRANSVERSE COHERENCE

The experimental apparatuses presented in the preceding section have been employed for the study of transverse coherence at BL19LXU; the coincidence enhancements R were measured as a function of slit width at $E = 14.41$ keV. First we present dependencies of R on the vertical slit widths w_y in Fig. 3. The measurements were done at two different slit positions $L = 66.7$ and 78.2 m. The horizontal beam size was restricted to 30 μm by the upstream slit ($L = 66.7$ m) for both cases. The total measurement time was 140 min for each condition. The coincidence profiles are well fitted by Eqs. (8) and (12) with two parameters: the coherence length σ_y and the scale factor $M_x M_t$. The obtained coherence lengths are $\sigma_y = 66.3 \pm 2.0$ and 77.5 ± 2.0 μm for $L = 66.7$ and 78.2 m, respectively. This result is consistent with the Van Cittert–Zernike theorem [28],

$$\sigma_y = \frac{\lambda L}{2\pi s_y}, \tag{17}$$

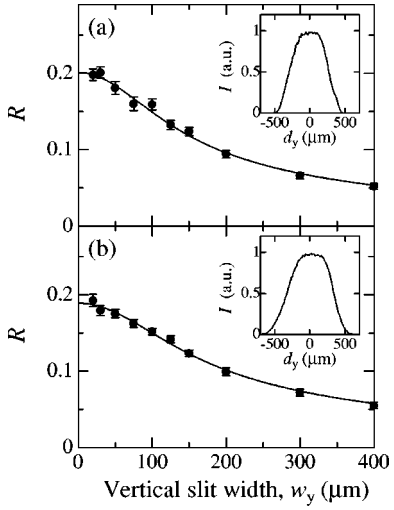

FIG. 3. R measured as a function of vertical slit width w_y. The slit position from the source is $L = 66.7$ m (a) and 78.2 m (b). Horizontal beamwidths are fixed at 30 μm by the slit at $L = 66.7$ m for both cases. The solid lines are the fitted curves based on Eqs. (8) and (12). The insets show vertical intensity profiles measured with scanning the slit (vertical slit width of 10 μm, central position of d_y).

which states the coherence length σ_y is proportional to the distance from the light source L. From Eq. (17) with our parameters, we determine the rms source size s_y to be 13.8 ± 0.4 μm. Note that s_y directly represents the electron beam size (i.e., not the convoluted size of electron beam and photon beam) in our case, where angular divergence of electron beam is sufficiently smaller than that of photon beam [46].

Next we performed similar measurements as a function of horizontal slit width w_x at different slit locations $L = 66.7$ and 78.2 m. The vertical beam sizes were limited to 50 μm by the upstream slit ($L = 66.7$ m). As shown in Figs. 4(a) and 4(b), we observed a significant difference between the coherence profiles at two conditions. First, the strong suppression of the peak enhancement ($\sim 26\%$) for the far-distance condition (b) was obtained. Second, R in Fig. 4(b) had an almost flat response with respect to w_x; the field becomes nearly coherent in horizontal. We also observed significant change of intensity profiles, as shown in the insets of Fig. 4.

Below we discuss origins for these unexpected phenomena. The suppression of the peak enhancement means an increase of the longitudinal mode number M_t (note that the transverse mode number M_y is kept same for both cases with the upstream slit). As expressed in Eq. (9), there are two possible reasons for the increase of M_t: a decrease of the longitudinal coherence time σ_t or an increase of the pulse width s_t. The former possibility can be easily checked by measuring energy resolution ΔE, because σ_t is represented using ΔE as in Eq. (10). After the measurement, we found ΔE at two conditions are same within our experimental accuracy; σ_t is unchanged. The result indicates that the pulse width s_t is elongated at the far-field condition.

We consider that the elongation originates from the asymmetric reflections in the HRM. The configuration of the

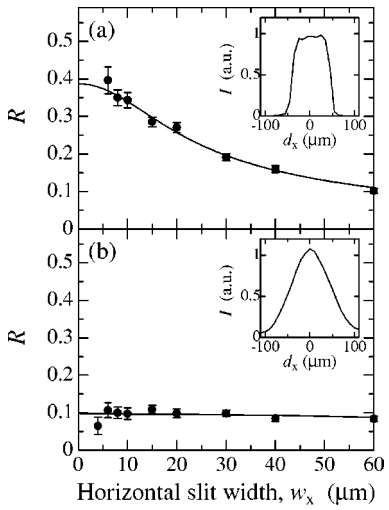

FIG. 4. R measured as a function of horizontal slit width w_y. The slit position from the source is $L=66.7$ m (a) and 78.2 m (b). Vertical beam widths are fixed at 50 μm by the slit at $L=66.7$ m for both cases. The solid lines are the fitted curves. The insets show horizontal intensity profiles measured with scanning the slit (horizontal slit width of 10 μm).

HRM produces a strong tilt of pulse envelop with respect to the propagation axis in the scattering plane [16,20,25,47], as schematically shown in Fig. 5(b). A simple geometrical consideration gives the tilt angle ψ just after the exit of the HRM as [20,48]

$$\tan\psi = 2\tan\theta_B(1/b+1)(1/b-1). \tag{18}$$

The temporal shift δ_t along the beam width δ_x is given by $(\delta_x \tan\psi)/c$. Now we take $\psi=89.954°$ from our geometry and $\delta_x \sim 60$ μm from the inset of Fig. 4(a). Then δ_t is estimated to be ~ 250 ps, which is much larger than the original width $s_t \sim 30$ ps [38]. After the free-space propagation of a distance l, the envelop becomes laterally broadened due to the angular divergence ($\omega_o = b^{-1/2}\omega_s = 6.5$ μrad), as in Fig. 5(c). Finally, the pulse width can approximate to δ_t for large l. We note that since the tilt of the pulse envelop diminishes the instantaneous lateral size as shown in Fig. 5(b), it is reasonable that the field becomes transversely coherent at the far field, as found in Fig. 4(b).

Although this naive model qualitatively explains the phenomena, there are still quantitative discrepancies from the experiment. For example, the expected pulse width $\delta_t \sim 200$ ps is almost twice as that experimentally given in Fig. 4(b). In addition, the obtained horizontal coherence length at the near location, $\sigma_x = 10.7$ μm [from Fig. 4(a)], does not coincide with the estimated value from the horizontal source size ($\sigma_x \sim 3$ μm), nor with that from the angular acceptance of the HRM ($\sigma_x \sim 5$ μm). A theory that treats coupling of transverse and longitudinal coherences in the dynamical diffraction [49] may help a more rigorous understanding of the phenomena. This kind of theory will be important especially for considering crystal optics that handles ultrafast x-ray pulses from XFELs.

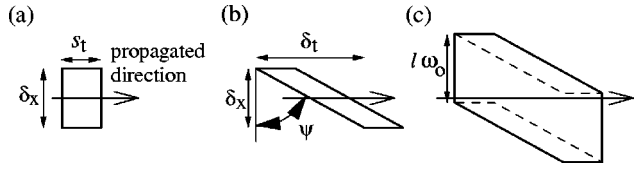

FIG. 5. Schematic view of pulse envelop before HRM (a), just after HRM (b), and after HRM with free-space propagation (c).

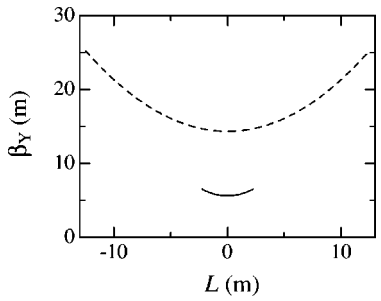

FIG. 6. Betatron functions for the 27 m undulator (dashed line) and for the 4.5 m undulator (solid line).

V. DETERMINATION OF SOURCE EMITTANCE

In the preceding section, we have determined vertical source size s_y. Now it is possible to evaluate the vertical emittance ϵ_y of the storage ring using a value of the betatron function β_y as

$$\epsilon_y = s_y^2/\beta_y. \tag{19}$$

The relationship, however, cannot be directly applied to our case, because the betatron function has a large variation along the long undulator, as shown in Fig. 6 [50] (i.e., the size $s_y = 13.8$ μm is only the average value along the undulator). A numerical simulation would be a possible choice for further analysis. However, a more direct approach is to measure with a shorter (4.5 m) undulator that has a more uniform betatron function, as seen in Fig. 6.

The experiment was done at BL29XU that is equipped with the 4.5 m undulator. Figure 7(a) shows R measured as a function of w_y at $L=53.3$ m. The measurement time for each point was same as before. Although the statistical errors increased due to the lack of brilliance, they are still small enough for quantitative analysis. From the fitting, the coherence length was determined to be $\sigma_y = 124.3 \pm 6.9$ μm, which corresponds to the source size of $s_y = 5.9 \pm 0.3$ μm. The vertical emittance was determined to be $\epsilon_y = 6.0 \pm 0.7$ pm rad from Eq. (19) with the mean value of the betatron function $\beta_y = 5.77$ m. Since the horizontal emittance at the experiment is evaluated to be $\epsilon_x = 6$ nm rad, the emittance coupling $\kappa = \epsilon_y/\epsilon_x$ is as small as 0.10%. It should be emphasized that our results show *instantaneous* values, because the effective time resolution is less than a nanosecond. Therefore it is natural that the values are smaller than that measured with visible Young's slit, where the resolving time is of the order of a millisecond [51].

Recently, low horizontal emittance operation ($\epsilon_x = 3$ nm rad) has been achieved at SPring-8 [52] by modify-

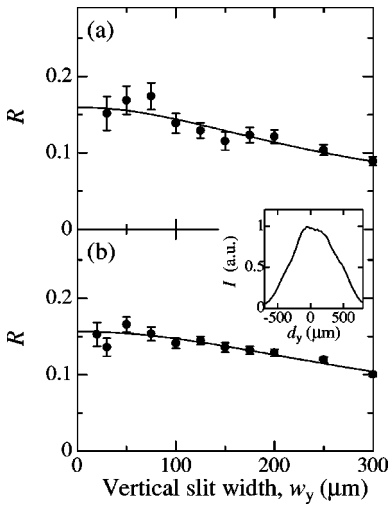

FIG. 7. R measured at BL29XU as a function of vertical slit width w_y with different source emittances $\epsilon_x = 6$ nm rad (a) and $\epsilon_x = 3$ nm rad (b). The distance to the slit is $L = 53.3$ m. The solid lines are the fitted curves. The inset shows a vertical intensity profile measured with scanning the slit (vertical slit width of 20 μm).

ing the dispersion function of the storage ring lattice [53,54]. It is important to investigate possible change of the vertical emittance at the low emittance operation. The result is shown in Fig. 7(b). The statistical errors are reduced due to the increase of brilliance. The following parameters are given by the fitting: $\sigma_y = 161.3 \pm 5.0$ μm, $s_y = 4.5 \pm 0.1$ μm (angular source size of 85 nrad), $\epsilon_y = 3.6 \pm 0.2$ pm rad, and $\kappa = 0.12\%$. We found that the coupling constant is kept almost same even at the low emittance operation.

Finally we discuss a resolution limit of our method. Because the radiation size from the single electron is $s_p \sim 1.6$ μm at $E = 14.41$ keV for the 4.5 m undulator [55], the resolution limit of s_y is estimated around 1 μm. Further improvement of the resolution is achieved by using higher-energy radiation (i.e., higher harmonics of undulator radiation). We can then evaluate s_y of submicron and ϵ_y of sub-pm rad.

VI. COHERENCE DEGRADATION BY PHASE OBJECT

Under coherent illumination, imperfect optical components possibly cause unwanted intensity modulations referred as speckles. Several x-ray optics can be harmful. First is transmission (refraction) optics, such as windows or filters [56,57]. Second is reflection optics, in particular, total reflection mirrors [58,59].

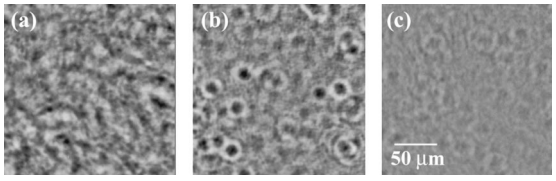

FIG. 8. Refractive contrast imaging of (a) graphite filter (sample A in Table I), (b) powder-foiled Be (sample B), and (c) ingot-foiled Be (sample C), taken at the 1 km station of BL29XU. These are in negative contrasts (black is high intensity). Details of experimental parameters are summarized in Table I.

Here we study coherence properties after transmission components (a graphite filter and Be windows), which are currently installed in our beam lines. The graphite filter, which absorbs unnecessary radiation in low energy, is retractable if desired, whereas three Be windows[2] cannot be removed because they are used for vacuum isolation.

As shown in Table I, a graphite filter (sample A) and a powder-foil Be window (sample B) were chosen as samples. For characterizing them, we took high-resolution images with an x-ray zooming tube [60] (lateral resolution of ~ 0.5 μm) under fully coherent illumination at the 1 km experimental station of BL29XU [61,62]. As a reference, we also took an image of a ingot-foil Be window (sample C), which is the same material as those installed in the beam lines for the coherence measurements in the previous sections. The images are shown in Fig. 8. Since the sample-to-camera distances were relatively large, the contrasts are mainly due to refraction in the samples. In the image of sample A, we observed irregular intensity modulations, which are caused by density fluctuations in the sample. The image of sample B shows a number of round-shaped spots being similar to the Airy patterns. It seems that these patterns originate partly from surface defects and partly from voids in the sample. The intensity distribution of the sample C was found to be much uniform.

Next we measured coherence profiles after installing the samples in the beam lines. The effect of the graphite (sample A) was studied at BL19LXU. The distance between the source to the sample is 45.5 m (see Fig. 1). The obtained profile in Fig. 9 shows a significant change from the original curve measured without the filter; the enhancement of R in the tail is much suppressed, and the central peak becomes sharp. The profile cannot be fitted with a single Gaussian coherence profile represented in Eq. (8). The fitting with double Gaussians gave much better agreement [37]. Additionally, the intensity profile measured with a vertical scan of the slit (a slit width of 10 μm) includes many speckles, as shown in the inset of Fig. 9.

Similarly, the effect of the poor-quality Be window (sample B) was investigated in BL29XU at the low-emittance operation. Two Be windows in the front-end (originally the same materials as the sample C) were replaced by the type-B windows. The source-to-window distance is 37.2 m. The measured coherence profile and intensity profile are shown in Fig. 10, which again show large changes from the original curves.

We discuss the origin of these transverse coherence degradations and criteria for coherence preservation. At first, it should be confirmed that any *stationary* object cannot degrade transverse coherence (i.e., $|\mu(\mathbf{x}_1;\mathbf{x}_2)| = 1$ for any $\mathbf{x}_1$

[2]Two windows are inserted between the front-end (ultrahigh vacuum) and the transport section (high vacuum), and one is between the transport section and the experimental station (atmosphere).

TABLE I. Sample characters and experimental conditions for refractive contrast imaging.

Sample no.	Material	Purity (%)	Roughness (Ra, μm)	Thickness (μm)	X-ray wavelength (nm)	Sample-to-camera distance (m)
A	Graphite[a]			100×9	0.086	1.8
B	Be (powder foil)	98.5	>1	250	0.10	1.5
C	Be (ingot foil)	99.8	0.1	250	0.10	1.5

[a]Density of 1 g/cm^3.

and $\mathbf{x}_2$) under two-dimensionally (both vertically and horizontally) coherent illumination [28]. In our case, however, good coherence is achieved only along one direction (vertical); horizontal coherence length is as small as a few microns at the object position.

We consider how a phase object affects coherence properties under such asymmetric situation. For the purpose, we treat the propagation law of transverse coherence function (mutual intensity) [28]. We represent the mutual intensity in front of the object as $J_i(\xi_1,\eta_1;\xi_2,\eta_2)$ and the correlation function of the object as $J_s(\xi_1,\eta_1;\xi_2,\eta_2) = P(\xi_1,\eta_1)P^*(\xi_2,\eta_2)$, where P is the transmittance amplitude function of the object. Note that the correlation function J_s is not a stochastically averaged function as usual (in Ref. [57], for example), but a deterministic one, because we treat a stationary object. The mutual intensity J_o at a distance z from the object is given by [28]

$$J_o(x_1,y_1;x_2,y_2)=\frac{1}{(\lambda z)^2}\int\int\int\int J_i(\xi_1,\eta_1;\xi_2,\eta_2) \times J_s(\xi_1,\eta_1;\xi_2,\eta_2)\exp\left[-\frac{i\pi}{\lambda z}((x_2-\xi_2)^2+(y_2-\eta_2)^2-(x_1-\xi_1)^2-(y_1-\eta_1)^2)\right] d\xi_1 d\eta_1 d\xi_2 d\eta_2 . \quad (20)$$

At first we consider a special condition for the incident beam: homogenous intensity with vertically coherent but horizontally incoherent field, i.e., $J_i(\xi_1,\eta_1;\xi_2,\eta_2) = \kappa I\delta(\xi_1-\xi_2)$. The propagated mutual intensity for vertically separated two points is represented as

$$J_o(x,y_1;x,y_2)=\frac{\kappa I}{(\lambda z)^2}\int\int\int J_s(\xi,\eta_1;\xi,\eta_2) \times\exp\left[-\frac{i\pi}{\lambda z}((y_2-\eta_2)^2-(y_1-\eta_1)^2)\right] \times d\xi d\eta_1 d\eta_2 . \quad (21)$$

Note that Eq. (21) is similar to that for one-dimensional mutual intensity after a moving object that is coherently illuminated, if we suppose the variable ξ stands for time. Therefore, it is clear from Eq. (21) that the fully vertical coherence in the incident beam can be destroyed after the object, if the correlation function $J_s(\xi,\eta_1;\xi,\eta_2)$ irregularly changes with respect to the horizontal position, ξ.

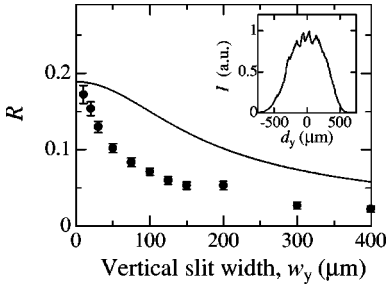

FIG. 9. R measured at BL19LXU as a function of vertical slit width w_y with a graphite filter (sample *A*). The solid line is the fitted curve without the filter shown in Fig. 3(b). The inset shows a vertical intensity profile measured with scanning the slit (vertical slit width of 10 μm).

For quantitative discussion, we performed numerical simulation of Eq. (20). A phase object is modeled based on the powder-foiled Be (sample *B*) as follows. We assume that the object[3] made of Be has a number of spherical holes that are randomly located over the object. We set a hole radius of $r=7$ μm and a density of $n=3000$ mm^{-2}, which are reasonable values from the image of Fig. 8(b) with Fresnel diffraction calculation [62]. The beam intensities onto the object are assumed to be Gaussian distributions with rms widths of 47 μm along both horizontal and vertical directions. The other parameters (source sizes of $s_x=274$ μm and $s_y=4.5$ μm, etc.) are same as those at the measurement for Fig. 10. The simulated mutual intensity was integrated based on Eq. (6) to get the vertical mode number. The result is shown in Fig. 10, where we found good agreement with the experimental result. Similarly, we performed calculation for sample *C*, assuming that the object has a number of hemispherical pits ($r=3$ μm) [62]. In this case, preservation of coherence was found to be nearly perfect, as is expected from the experimental results in the previous sections. In addition, calculations for horizontal coherence do not show significant degradation in both cases, because the horizontal coherence length is smaller than the typical correlation lengths of the phase objects.

In these examples, we used some models for representing transmittance functions P of the objects. However, more rig-

[3]A departure of refractive index from unity is $\delta_r=-1.6\times10^{-6}$ at $E=14.41$ keV, from Ref. [65]. Absorption was neglected.

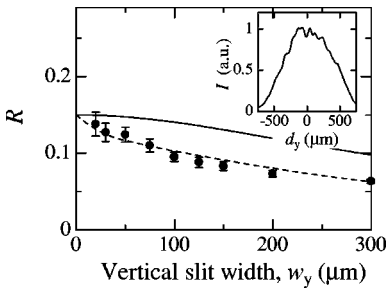

FIG. 10. *R* measured at BL29XU as a function of vertical slit width w_y after replacing the front-end Be windows (sample *C*) by type-*B* ones. The solid line is the fitted curve with the type-*C* windows shown in Fig. 7(b), after a slight modification of the scale factor. The dashed line is a simulated result (see text). The inset shows a vertical intensity profile measured with scanning the slit (vertical slit width of 20 μm).

orous function can be obtained from propagation-based method [4,5] or sharing interferometric method [63] in high-lateral resolution. Then we can evaluate coherence properties more accurately.

This procedure can be easily applied to treating reflection optics. The reflectance amplitude function of the mirror can be given by accurate measurement of surface figure [58] or coherent imaging with iterative calculations [59]. Qualitatively, it is expected that condition of coherence preservation in this case is not so severe as that for transmission optics, because phase modulation is approximated in one dimensional due to the grazing incidence condition.

VII. CONCLUSION

We have studied coherence properties of synchrotron radiation with x-ray intensity interferometry. Transverse coherence profiles were determined from the measurements of mode numbers as functions of slit widths. The relationship between the coherence length in vertical (a direction perpendicular to the scattering plane of HRM) and the distance is consistent with the Van Cittert–Zernike theorem, whereas that in horizontal (in the scattering plane) shows an unexpected behavior, which may be caused by the tilt of pulse envelop in the scattering plane. From the coherence measurements, we have accurately determined vertical emittances of the storage ring. The resulting value at the low-emittance operation is as small as $\epsilon_y = 3.6 \pm 0.2$ pm rad. The resolution can be further improved by the use of higher-energy radiation. We have studied coherence degradations with optical components such as a graphite filter and different types of Be windows. We showed that it is important to know a stationary transmittance amplitude function of the object for accurate determination of coherence properties of the wave field after the object.

ACKNOWLEDGMENTS

The authors thank Dr. S. Goto and Dr. S. Takahashi for providing the Be windows and the graphite filters; Dr. H. Tanaka, Dr. M. Takao, and Dr. K. Soutome for accelerator operation at the emittance measurement; and Professor E. Ikonen for fruitful discussion and careful reading of the manuscript. One of the authors (M.Y.) is grateful to Professor Y. Amemiya for extensive discussion.

[1] M. Sutton, S.G.J. Mochrie, T. Greytak, S.E. Nagler, L.E. Berman, G.A. Held, and G.B. Stephenson, Nature (London) **352**, 608 (1991).
[2] S. Brauer, G.B. Stephenson, M. Sutton, R. Brüning, E. Dufresne, S.G.J. Mochrie, G. Grübel, J. Als-Nielsen, and D.L. Abernathy, Phys. Rev. Lett. **74**, 2010 (1995).
[3] S.B. Dierker, R. Pindak, R.M. Fleming, I.K. Robinson, and L. Berman, Phys. Rev. Lett. **75**, 449 (1995).
[4] A. Snigirev, I. Snigireva, V. Kohn, S. Kuznetsov, and I. Schelokov, Rev. Sci. Instrum. **66**, 5486 (1995).
[5] P. Cloetens, R. Barrett, J. Baruchel, J.P. Guigay, and M. Schlenker, J. Phys. D **29**, 133 (1996).
[6] K.A. Nugent, T.E. Gureyev, D.F. Cookson, D. Paganin, and Z. Barnea, Phys. Rev. Lett. **77**, 2961 (1996).
[7] P. Cloetens, W. Ludwig, J. Baruchel, D.V. Dyck, J.V. Landuyt, J.P. Guigay, and M. Schlenker, Appl. Phys. Lett. **75**, 2912 (1999).
[8] J. Miao, P. Charalambous, J. Kirz, and D. Sayre, Nature (London) **400**, 342 (1999).
[9] I.K. Robinson, I.A. Vartanyants, G.J. Williams, M.A. Pfeifer, and J.A. Pitney, Phys. Rev. Lett. **87**, 195505 (2001).
[10] J. Miao, T. Ishikawa, B. Johnson, E.H. Anderson, B. Lai, and K.O. Hodgson, Phys. Rev. Lett. **89**, 088303 (2002).
[11] G.J. Williams, M.A. Pfeifer, I.A. Vartanyants, and I.K. Robinson, Phys. Rev. Lett. **90**, 175501 (2003).
[12] K. Yamauchi, K. Yamamura, H. Mimura, Y. Sano, A. Saito, A. Souvorov, M. Yabashi, K. Tamasaku, T. Ishikawa, and Y. Mori, J. Synchrotron Radiat. **9**, 313 (2002).
[13] The LCLS Design Study Group, Stanford Linear Accelerator Center (SLAC), Report No. SLAC-R-521, 1998 (unpublished).
[14] DESY, Report No. DESY97-048, edited by R. Brinkmann, G. Materlik, J. Rossbach, and A. Wagner, 1997 (unpublished).
[15] T. Shintake *et al.*, Nucl. Instrum. Methods Phys. Res. A **507**, 382 (2003).
[16] T. Ishikawa, Acta Crystallogr., Sect. A: Found. Crystallogr. **44**, 496 (1988).
[17] A.Q.R. Baron, A.I. Chumakov, H. Grünsteudel, H. Grünsteudel, L. Niesen, and R. Rüffer, Phys. Rev. Lett. **77**, 4808 (1996).
[18] K. Fezzaa, F. Comin, S. Marchesini, R. Coïsson, and M. Belakhovsky, J. X-Ray Sci. Technol. **7**, 12 (1997).
[19] P. Cloetens, J. Guigay, C.D. Martino, J. Baruchel, and M. Schlenker, Opt. Lett. **22**, 1059 (1997).
[20] H. Yamazaki and T. Ishikawa, Proc. SPIE **2856**, 279 (1996).
[21] K. Tamasaku and T. Ishikawa, Acta Crystallogr., Sect. A: Found. Crystallogr. **57**, 197 (2000).
[22] V. Kohn, I. Snigireva, and A. Snigirev, Phys. Rev. Lett. **85**, 2745 (2000).
[23] J.J.A. Lin *et al.*, Phys. Rev. Lett. **90**, 074801 (2003).
[24] A. Appel and U. Bonse, Phys. Rev. Lett. **67**, 1673 (1991).
[25] K. Izumi, T. Mitsui, M. Seto, Y. Yoda, T. Ishikawa, X.-W. Zhang, M. Ando, and S. Kikuta, Jpn. J. Appl. Phys., Part 1 **34**, 5862 (1995).

[26] K. Fezzaa and W.-K. Lee, J. Appl. Crystallogr. **34**, 166 (2001).
[27] R. Hanbury Brown and R.Q. Twiss, Nature (London) **177**, 27 (1956).
[28] J.W. Goodman, *Statistical Optics* (Wiley, New York, 1985).
[29] É.V. Shuryak, Zh. Éksp. Teor. Fiz. **67**, 60 (1974) [Sov. Phys. JETP **40**, 30 (1975)].
[30] E. Ikonen, Phys. Rev. Lett. **68**, 2759 (1992).
[31] Y. Kunimune, Y. Yoda, K. Izumi, M. Yabashi, X.-W. Zhang, T. Harami, M. Ando, and S. Kikuta, J. Synchrotron Radiat. **4**, 199 (1997).
[32] E. Gluskin, E.E. Alp, I. McNulty, W. Sturhahn, and J. Sutter, J. Synchrotron Radiat. **6**, 1065 (1999).
[33] R.Z. Tai, Y. Takayama, N. Takaya, T. Miyahara, S. Yamamoto, H. Sugiyama, J. Urakawa, H. Hayano, and M. Ando, Phys. Rev. A **60**, 3262 (1999).
[34] Y. Takayama, H. Sugiyama, T. Yoshida, C. Lee, K. Obu, H. Otsubo, T. Miyahara, S. Yamamoto, and M. Ando, J. Synchrotron Radiat. **10**, 303 (2003).
[35] T. Tanabe, M.C. Teich, T.C. Marshall, and J. Galayda, Nucl. Instrum. Methods Phys. Res. A **304**, 77 (1991).
[36] M. Yabashi, K. Tamasaku, S. Kikuta, and T. Ishikawa, Rev. Sci. Instrum. **72**, 4080 (2001).
[37] M. Yabashi, K. Tamasaku, and T. Ishikawa, Phys. Rev. Lett. **87**, 140801 (2001).
[38] M. Yabashi, K. Tamasaku, and T. Ishikawa, Phys. Rev. Lett. **88**, 244801 (2002).
[39] T. Hara, M. Yabashi, T. Tanaka, T. Bizen, S. Goto, X.M. Maréchal, T. Seike, K. Tamasaku, T. Ishikawa, and H. Kitamura, Rev. Sci. Instrum. **73**, 1125 (2002).
[40] K. Tamasaku, M. Yabashi, D. Miwa, T. Mochizuki, and T. Ishikawa, Proc. SPIE **4782**, 132 (2002).
[41] E. Ikonen and R. Rüffer, Hyperfine Interact. **92**, 1089 (1994).
[42] J. Krzywinski, E.L. Saldin, E.A. Schneidmiller, and M.V. Yurkov, Nucl. Instrum. Methods Phys. Res. A **401**, 429 (1997).
[43] M. Yabashi *et al.*, Nucl. Instrum. Methods Phys. Res. A **467–468**, 678 (2001).
[44] K. Tamasaku, Y. Tanaka, M. Yabashi, H. Yamazaki, N. Kawamura, M. Suzuki, and T. Ishikawa, Nucl. Instrum. Methods Phys. Res. A **467–468**, 686 (2001).
[45] A.Q.R. Baron, Hyperfine Interact. **125**, 29 (2000).
[46] R. Coïsson, Appl. Opt. **34**, 904 (1995).
[47] E. Ikonen, Phys. Rev. A **66**, 065802 (2002).
[48] E. Ikonen (private communication).
[49] H. Yamazaki and T. Ishikawa, J. Appl. Crystallogr. **36**, 213 (2003).
[50] H. Tanaka, K. Soutome, M. Takao, M. Masaki, H. Ohkuma, K. Kumagai, and J. Schimizu, Nucl. Instrum. Methods Phys. Res. A **486**, 521 (2002).
[51] M. Masaki and S. Takano, J. Synchrotron Radiat. **10**, 295 (2003).
[52] H. Ohkuma *et al.*, in *Proceedings of the 2003 Particle Accelerator Conference, Portland, 2003*, edited by J. Chew, P. Lucas, and S. Webber (IEEE Operations Center, Piscataway, NJ, 2003), p. 881.
[53] L. Farvacque, J.L. Laclare, P. Nghiem, J. Payet, A. Ropert, H. Tanaka, and A. Tkatchenko, in *Proceedings of the 4th European Particle Accelerator Conference*, (World Scientific, Singapore, 1994), p. 612.
[54] Å. Andersson, M. Eriksson, L.J. Lindgren, P. Rösel, and S. Werin, in Proceedings of the 4th European Particle Accelerator Conference (World Scientific, Singapore, 1994), p. 588.
[55] T. Tanaka and H. Kitamura, J. Synchrotron Radiat. **8**, 1221 (2001).
[56] A. Snigirev, I. Snigireva, V.G. Kohn, and S.M. Kuznetsov, Nucl. Instrum. Methods Phys. Res. A **370**, 634 (1996).
[57] I.A. Vartanyants and I.K. Robinson, Opt. Commun. **222**, 29 (2003).
[58] Y. Mori *et al.*, Proc. SPIE **4501**, 30 (2001).
[59] A. Souvorov, M. Yabashi, K. Tamasaku, T. Ishikawa, Y. Mori, K. Yamauchi, K. Yamamura, and A. Saito, J. Synchrotron Radiat. **9**, 223 (2002).
[60] T. Matsumura, K. Kinoshita, S. Tamura, N. Kamijyo, Y. Ozaki, and H. Kihara, in *X-ray Microscopy and Spectromicroscopy*, edited by J. Thieme, G. Schmahl, D. Rudolph, and E. Umbach (Springer-Verlag, Berlin, 1998), p. II-195.
[61] T. Ishikawa *et al.*, Proc. SPIE **4145**, 1 (2001).
[62] S. Goto, M. Yabashi, K. Tamasaku, S. Takahashi, and T. Ishikawa (unpublished).
[63] Y. Kohmura, T. Ishikawa, H. Takano, and Y. Suzuki, J. Appl. Phys. **93**, 2283 (2002).
[64] K. Tamasaku, M. Yabashi, and T. Ishikawa, Appl. Phys. Lett. **83**, 2994 (2003), and references therein.
[65] B.L. Henke, E.M. Gullikson, and J.C. Davis, At. Data Nucl. Data Tables **54**, 181 (1993).